Optimal Voltage Regulator for Inverter Interfaced Distributed Generation Units Part I: Control System

Mohsen Eskandari, Li Li, *Member, IEEE,* Mohammad Hassan Moradi, Pierluigi Siano, *Senior Member, IEEE,* Frede Blaabjerg, *Fellow, IEEE*

Abstract- The stable operation of conventional power systems greatly depends on coherent impedances of the bulk power networks' elements. However, penetration of inverter interfaced distributed generation (IIDG) units put the stability of modern power systems into a risk due the vague and arbitrary output impedance of IIDG units. Besides, the impedance specification of IIDGs can only be established by means of a virtual impedance loop, which needs extra control efforts also imposes voltage drops. Especially, the virtual impedance depends on the output current and cannot be thus freely adjusted. To this end, an optimal voltage regulator (OVR) is proposed for controlling IIDG units to achieve a free/wide range of impedance shaping. The OVR facilitates the optimal impedance shaping based on the control requirement and grid's impedance characteristics, which makes the IIDG units consistent with the power network thus contributing to stabilizing modern power systems. The OVR's control system is based on the state feedback control and the impedance shaping is achieved through an appropriate feedback gain adjustment process. Simulation results prove the effectiveness of the method to achieve the desired impedance shaping.

***Index Terms*—Impedance shaping, Inverter interfaced distributed generation (IIDG), Microgrid (MG), Optimal control, State feedback control.**

I. Introduction

THE development in the semiconductors field has encouraged power engineers to integrate renewable energy resources (RESs), micro-power sources and energy storage systems as distributed generation (DG) units into the power system at a large scale [1]-[2]. DG units are connected to ***ac*** grids via power converter-based interfaces, called inverters. Various control strategies have been proposed for inverters such as proportional–integral (PI) control [3], proportional–resonant (PR) control [4], robust servomechanism control [5], nonlinear control [6]-[9], model predictive control [10]-[11], linear quadratic Gaussian control [12], synchronverter [13], servo-voltage source inverter (VSI) [14]. These control methods have been designed based on the inverters' application in the power system and mainly for voltage and frequency regulation, load feeding and grid supporting [15].

However, the main issue, which has been a key to the stable operation of conventional bulk power systems, i.e. the *harmony* inherently existing in the conventional power systems, has not been appropriately considered in developing these methods. The *harmony* exists due to *the inductivity of conventional power systems' elements* at all levels, i.e. generation, transmission and even the loads[1]. In other words, *the consistency of impedance characteristics of all elements in realizing/decoupling* the frequency-active power (*f*-*P*) and voltage-reactive power (*V*-*Q*) control systems implemented at synchronous machines leads to the desired *harmony*.

On the other hand, the low/medium voltage grids, which are the cradle of inverter-interfaced DG (IIDG) units, possess different inductivity/resistivity (X/R ratio) characteristics. Besides, the output impedance of IIDG units, which is greatly affected by their control system [16], diffuse into the grid and thus is critically/dominantly effective [17]. Moreover, the microgrid (MG) concept has gained full attention to improve the supply reliability to sensitive loads with autonomous operation capability [18]-[19]. The droop controlled IIDG units are responsible for grid (voltage and frequency) forming as well as for active and reactive load supporting in low/medium voltage MGs [20]. Now, the question is how harmony can be established in modern power systems including grid-connected IIDGs or in an autonomous MG as being a small-scale power system, so that a stable operation can be achieved.

The synchronverter is developed in [13] to mimic the dynamic response of synchronous generators while designing inverters' control system, in order to give a sense of coherence to the modern power systems. However, it is argued that including the swing equation in the control system of inverters is a promising solution to deal with the stability issue of modern power systems. As the swing equation in synchronous machines comes from the natural inertia of the rotor mass, this inertia prevents sudden changes in frequency and thus smooths the disturbances inserted into the system, meanwhile the energy stored in the rotor mass meets sudden load changes. So, including the virtual inertia into the control system of an inverter, without providing a coordinated spinning reserve for load changes is not always an advantage since it makes the power control loop more complicated. Although the synchronverter establishes the *f*-*P* relation in the IIDG's control system, the impedance characteristics of the interconnecting power lines do not meet the control requirement. For this reason, the impedance shaping is important and the synchronverter also needs a virtual impedance loop for impedance shaping, to improve its dynamics [21]. Besides, *f*-*P* relation can be easily implemented by conventional *f*-*P* droop loops and the

[1] Induction machines dominantly constitute the loads in distribution systems which makes the nature of distribution grids inductive. That's why the VAr compensators are extensively installed at sub-stations, yet, they do not operate at unit power factor to avoid resonances with inductive elements.

virtual inertia is already included in the control system of inverters using low-pass filters [22]. Moreover, energy storage systems like batteries and super-capacitors provide spinning reserve to the system [23]-[24].

So, in order to achieve the desired *harmony*, the impedance shaping is vital to satisfy the impedance characteristics required to establish the decoupled *f-P* and *V-Q* relations and to avoid cross-coupling between control loops, which critically impacts the stability of power systems [25]. Impedance shaping has been considered as a promising solution to identify and improve the dynamic performance of IIDG units in modern power systems [26]-[28], and some stability criteria for impedance specification have been proposed [29]-[34]. However, the only consideration of impedance shaping in the inverters' control system is achieved through a virtual impedance loop over the existing inner control loops of inverters [35]-[36]. On the other hand, the virtual impedance causes some problems like voltage drop, voltage band limits, extra control loops/efforts and limited maximum transferable power [37]. Moreover, all control objectives cannot be satisfied via solely using a virtual impedance loop, and its performance depends on the output current [38]. Moreover, the low/medium power networks have their own impedance characteristics, which must be considered for the output impedance design of inverters [17] to achieve a stabilizing *harmony* in the modern power system or in an autonomous MG. Therefore, in order to void complexity of the modern power systems while preserving consistency of the output impedance characteristics of IIDG units with the grid and the control targets, a novel control system is proposed in this paper, which enables a wide range of freedom for impedance specification. The novel contributions of the proposed method are as follows:

- An optimal voltage regulator (OVR) based on the state feedback control as a voltage source to be adopted for controlling IIDG units in the modern power system. The state feedback loop facilitates the desired output impedance shaping for the OVR through selecting appropriate state feedback gains. The OVR includes only one integrator, in comparison to PI-based VSIs with four integrators.
- The linear quadratic (optimal) regulator (LQR) is employed to determine the feedback gain matrix. Nevertheless, the LQR performance is critically affected by the index matrices. Therefore, a nonlinear multi-objective cost function based on the OVR's output impedance shaping (dynamic performance) as well as its robustness in disturbance rejection is proposed to determine the optimum index matrices.
- Moreover, a Pareto quantum particle swarm optimization (PQ-PSO) method is developed to address the nonlinearity and multi-objective of the cost function in order to optimally tune the OVR parameters (state feedback gains).

In the second part of the paper, the application of the OVR to develop a universal model for both the grid-connected (grid-feeding) and as a grid-forming inverter in autonomous MGs, also exposed to unbalanced/harmonics conditions, is examined while considering optimal impedance shaping.

In the next section, the control system of the conventional VSI is elaborated. The OVR is proposed and designed in Section III. Numerical and simulation results are presented in Section IV. Finally, conclusions are presented in Section V.

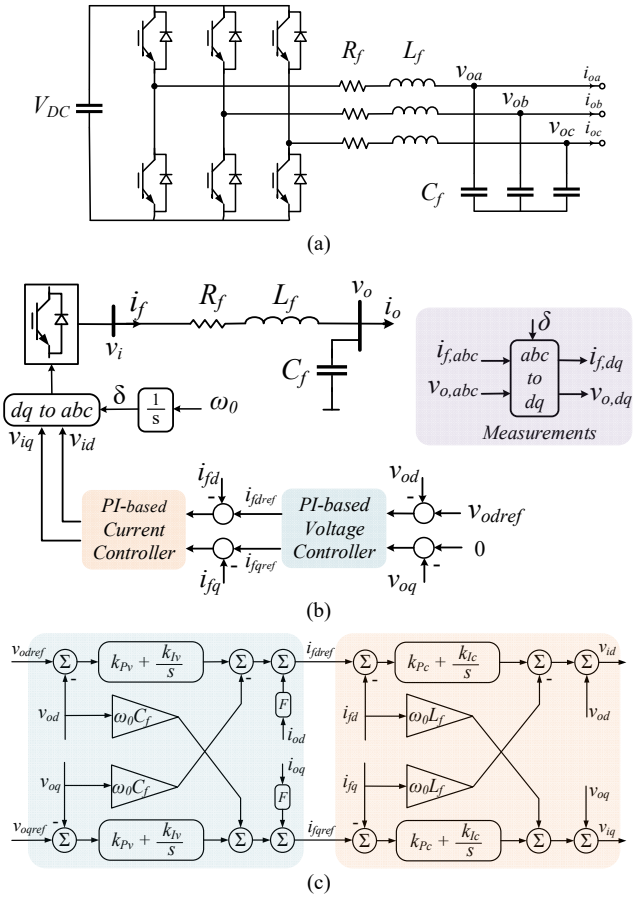

Fig. 1. Voltage source inverter (grid forming): (a) electrical circuit; (b) single phase diagram and control system; (c) the inner control loops.

II. Voltage Source Inverter

A. Conventional Control System

A schematic diagram of the electrical circuit and the control system of the VSI is depicted in Fig. 1. The electrical part of the VSI is composed of three parts: the DC link, which is provided by the primary resource, the three-phase power converter (including pulse width modulation (PWM) and semiconductor switches), and the LC filter for removing high frequency switching ripples from the output waveform.

The dynamics of a VSI can be categorized into two major groups regarding their time constants: 1) dynamics related to the fast switching process through PWM unit and switches; 2) dynamics related to the DC link and LC filter and VSIs inner control loops. The VSIs inner control loops are embedded in the system in order to modify the LC filter dynamics and to compensate for voltage fluctuations at the DC link [15], and thus critically affect the dynamic response of the VSIs. In this sense, the dynamics and nonlinearity arose from the first group of events which, as stated above, are normally neglected in the studies carried out in the context of the second group due to the different time scales [39]. The control system of the VSI including the inner PI-based controllers, implemented in the *d-q* synchronous reference frame, are demonstrated in Fig. 1(b) and (c), respectively [15].

B. VSI Output Impedance

The output impedance of the VSI is developed to investigate the impact of the control system on the VSI's dynamic performance. The VSI output voltage is given from Kirchhoff's voltage law (KVL) as:

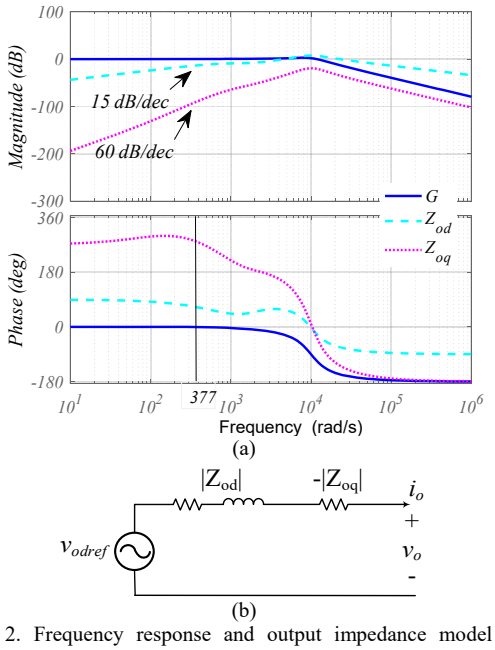

Fig. 2. Frequency response and output impedance model of the conventional PI-based VSI: (a) bode plot of the VSI's output impedance; (b) equivalent circuit model.

$$v_{od} = -\left(R_f + s\,L_f\right) i_{fd} + L_f\,\omega_0\,i_{fq} + v_{id} \tag{1}$$

$$v_{oq} = -\left(R_f + s\,L_f\right) i_{fq} - L_f\,\omega_0\,i_{fd} + v_{iq} \tag{2}$$

where v_{od} & v_{oq} are the *d-q* components of the output voltage (over the LC filter capacitor), R_f & L_f represent the resistance and inductance of the LC filter inductor, i_{fd} & i_{fq} are the *d-q* component of the LC filter current, s is the Laplace operator and ω_0 is the electrical angular frequency. v_{id} and v_{iq} are the *d-q* components of the input voltage to the power converter, which are determined by the current controller. The power converter is modeled as a unit gain because of the very fast dynamics of the switching process. The current controller (inner loop) for determining the input voltage is modelled as:

$$v_{id} = -\omega_0\,L_f\,i_{fq} + \left(k_{Pc} + \frac{k_{Ic}}{s}\right)\left(i_{fdref} - i_{fd}\right) + v_{od} \tag{3}$$

$$v_{iq} = \omega_0\,L_f\,i_{fd} + \left(k_{Pc} + \frac{k_{Ic}}{s}\right)\left(i_{fqref} - i_{fq}\right) + v_{oq} \tag{4}$$

where k_{Pc} & k_{Ic} are the proportional and integral gains of the current control loop, respectively, i_{fdref} & i_{fqref} are the *d-q* components of the reference currents determined by the voltage controller (outer loop). The voltage controller is modelled as (note that $v_{oqref} = 0$):

$$i_{fdref} = F\,i_{od} - \omega_0\,C_f\,v_{oq} + \left(k_{Pv} + \frac{k_{Iv}}{s}\right)\left(v_{odref} - v_{od}\right) \tag{5}$$

$$i_{fqref} = F\,i_{oq} + \omega_0\,C_f\,v_{od} + \left(k_{Pv} + \frac{k_{Iv}}{s}\right)\left(-v_{oq}\right) \tag{6}$$

where k_{Pv} & k_{Iv} are the proportional and integral gains of the voltage control loop, respectively, and F is the feedforward gain. The currents i_{fd} & i_{fq} are given from Kirchhoff's current law (KCL) as:

$$i_{fd} = C_f\,s\,v_{od} - C_f\,\omega_0\,v_{oq} + i_{od} \tag{7}$$

$$i_{fq} = C_f\,s\,v_{oq} + C_f\,\omega_0\,v_{od} + i_{oq} \tag{8}$$

Table I. Electrical and control parameters of PI-based VSI

LC filter	R_f	L_f	C_f
	0.1 Ω	1e-3 H	50e-6 F
Voltage control loop	k_{Pv}	k_{Iv}	F
	0.5	390	0.75
Current control loop	k_{Pc}	k_{Ic}	-
	10.5	16000	-
Power Converter	ω_s	Rated power	Voltage (L-L)
	8 kHz	30 kW	400 V

From (1)-(8) and by eliminating v_{oq}, the output voltage is given as:

$$v_o = G(s)\,v_{odref} - Z_{od}(s)\,i_{od} - Z_{oq}(s)\,i_{oq} \tag{9}$$

A detailed version of (9) is given in Appendix A. The bode plots of $G(s)$, $Z_{od}(s)$ and $Z_{oq}(s)$ for a VSI with electrical and control parameters in Table I given from [39], are shown in Fig. 2. The phasor of $G(s)$ is $1\angle 0^o$, at the low frequencies. Therefore, it can be modeled as an ideal voltage source equal to v_{odref}. The phasor of Z_{od} at the operating angular frequency (ω_0=377 rad.s^{-1}) is $0.2\angle 65^o$, with the X/R ratio of the output impedance around 2. The phase angle of Z_{oq} is roughly 280°. Taking into consideration that the phase angle of i_{oq} is -90° (i_{oq} is negative for positive output reactive power), so $Z_{oq}\,i_{oq}$ can be modeled as a negative resistance. The equivalent circuit model of VSI is depicted in Fig. 2(b).

Two issues should be considered in the equivalent circuit model[2]: ***a)*** although the ideal voltage source, v_{odref}, is located behind the output impedance, the output current does not cause a voltage drop over the output impedance that means v_o=v_{odref} in the steady states. In other words, the inverter is intended to follow the reference voltage (v_{odref}) at its output and the output impedance specifies the voltage dynamics when it approaches to the reference value. So, although the VSI's output impedance (affected by the inner control loops) does not cause a real voltage drop, it impacts on the inverter's dynamic performance. However, if the conventional virtual impedance loop is adopted to boost the output impedance of the VSI, the voltage drop would be realistic, which is a drawback of the virtual impedance loop; ***b)*** i_o is considered to be aligned to the i_{od}'s direction, so, although the unit of $Z_{oq}\,i_{oq}$ is voltage, its negative sign comes from a negative resistance mapped to the direct axis. Nevertheless, the magnitude of the equivalent output impedance at the operating frequency is small ($|Z_{od}|$=0.2 and $|Z_{oq}|$=3.2e-5) and it can be ignored.

In this way, the VSI can be modeled as an ideal voltage source, but, it is not advantageous from both practical, control and operational, points of view for the following reasons:

1) Power converters expose low current limits and low output impedance causes large current in transients. Although adopting a current limiter in the current control loop of PI-based VSI is a solution, this influences the dynamic performance of the VSI and significantly destroys the dynamic stability of networked MGs due to different characteristic of VSIs in current limiting mode [16]. Besides, insufficiency of the PI current controller with a limiter in the presence of unbalanced faults or unbalanced loading condition is a matter of concern. Although extra loops can be utilized for negative sequence to address the problem [40], it adds more integrators and makes the

[2] These items are presented to explain Fig. 2(b) and are not general arguments. Fig. 2(b), and later in this paper Fig. 5(d), are presented for the reader to have an intuition about the output impedance of IIDG units and how it affects the dynamic performance of IIDG units in the electrical circuit.

stability margin much worse and the control system more complex in terms of stability analysis.

2) The inductive output impedance of IIDG units helps the control system to have better performance and dynamic stability in droop-based networked MGs [17], [42]. Some researchers have relied on the output impedance of VSI, which inherently is provided by the VSI control system [43]. However, the output impedance of a PI-based is not effective for enhancing the X/R ratio of the feeder, seen from VSI in order to decouple the typically used *f-P* and *V-Q* droop control loops in autonomous MGs. Besides, the output impedance of the PI-based VSI cannot freely be adjusted by selecting the PI gains. Moreover, adopting the extra virtual impedance loops, over the VSI's inner control loops, imposes disadvantages such as voltage drop, extra control effort, and power transfer limit.

3) In conventional voltage sources like synchronous generators, the series output impedance causes voltage drop in fault situations and limits the fault currents. More importantly, fixed inductive output impedance of the synchronous generators, even in the fault conditions, helps to develop the directional protection schemes. On the other hand, VSIs reveal different output impedance characteristics when they switch to the current limiting mode [16], which is not fully controllable. It is not beneficial in the fault situations as a novel protection scheme as well as new protection relaying is required [44].

In the next section, the OVR is developed to overcome the drawbacks of the conventional VSIs, which are mentioned earlier.

III. Optimal Voltage Regulator (OVR)

Schematic diagram of the proposed OVR is depicted in Fig. 3. In comparison to the conventional VSI, which includes four integrators for the inner loops, the proposed OVR includes only one integrator. The integrator loop operates in parallel with the state feedback loop and drives the *d* component of the output voltage to the reference value determined by the outer power/droop control loop. The state feedback loop is adopted to move the system poles to the desired locations to obtain the desirable impedance shaping as a criteria of dynamic performance and stability.

This is implemented by tuning the state feedback gain matrix. In this regard, the LQR method is adopted [45]. For a controllable system with a typical state space model as:

$$\dot{x} = A\,x + B\,u \tag{10}$$

the LQR method determines the state feedback matrix K in:

$$u = -K\,x \tag{11}$$

so as to minimize the following performance index:

$$J = \int \left(x^{*} Q\,x + u^{*} R\,u\right) dt \tag{12}$$

where x is the state variable matrix, A and B are the state and input matrices, respectively, and u specifies the control inputs.

The matrices Q & R are semi-positive-definite and positive-definite real symmetric matrices respectively, which conventionally compromise the dynamic response and steady state accuracy (control effort or energy from the control signal). Then the matrix K is developed as:

$$K = R^{-1} B^{*} P \tag{13}$$

where the semi-positive-definite stabilizing matrix P satisfies the Riccati equation as:

$$A^{*} P + PA - PBR^{-1} B^{*} P + Q = 0 \tag{14}$$

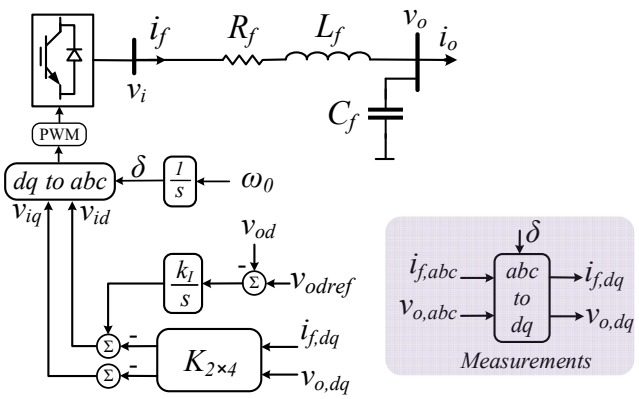

Fig. 3. The proposed control system for OVR.

The matrices Q & R significantly influence the determination of the feedback gain matrix K and consequently the performance of the OVR, which is not yet well established in the literature especially in the case of IIDGs. In the case of the OVR proposed in this work, Q & R are optimally determined through an optimization process. To this end, the state space model as well as output impedance of the OVR should be developed.

A. OVR State Space Model

The state variables related to the LC filter, i.e. the *d-q* components of the LC filter current (i_{fd} & i_{fq}) and output voltage (v_{od} & v_{oq}) are given as:

$$\dot{i}_{fd} = -\frac{R_f}{L_f} i_{fd} + \omega_0\, i_{fq} + \frac{1}{L_f} v_{id} - \frac{1}{L_f} v_{od} \tag{15}$$

$$\dot{i}_{fq} = -\frac{R_f}{L_f} i_{fq} - \omega_0\, i_{fd} + \frac{1}{L_f} v_{iq} - \frac{1}{L_f} v_{oq} \tag{16}$$

$$\dot{v}_{od} = \omega_0 v_{oq} + \frac{1}{C_f} i_{fd} - \frac{1}{C_f} i_{od} \tag{17}$$

$$\dot{v}_{oq} = -\omega_0\, v_{od} + \frac{1}{C_f} i_{fq} - \frac{1}{C_f} i_{oq} \tag{18}$$

The state space model representing the LC filter is developed as:

$$\begin{aligned} \dot{x}_{LC} &= A_{LC}\; x_{LC} + B_{LCIV}\; \Delta u_{LCIV} + B_{LCOC}\; \Delta u_{LCOC} \\ y_{LC} &= C_{LC}\, x_{LC} \end{aligned} \tag{19}$$

where $x_{LC} = \left[\Delta i_{fd} \quad \Delta i_{fq} \quad \Delta v_{od} \quad \Delta v_{oq}\right]^T$

$$u_{LCIV} = \left[\Delta v_{id} \quad \Delta v_{iq}\right]^T,\; u_{LCOC} = \left[\Delta i_{od} \quad \Delta i_{oq}\right]^T,\; y_{LC} = \Delta v_{od}$$

$$A_{LC} = \begin{bmatrix} \frac{-R_f}{L_f} & \omega_0 & \frac{-1}{L_f} & 0 \\ -\omega_0 & \frac{-R_f}{L_f} & 0 & \frac{-1}{L_f} \\ \frac{1}{C_f} & 0 & 0 & \omega_0 \\ 0 & \frac{1}{C_f} & -\omega_0 & 0 \end{bmatrix},\; B_{LCIV} = \begin{bmatrix} \frac{1}{L_f} & 0 \\ 0 & \frac{1}{L_f} \\ 0 & 0 \\ 0 & 0 \end{bmatrix},\; B_{LCOC} = \begin{bmatrix} 0 & 0 \\ 0 & 0 \\ \frac{-1}{C_f} & 0 \\ 0 & \frac{-1}{C_f} \end{bmatrix}$$

$$C_{LC} = \begin{bmatrix} 0 & 0 & 1 & 0 \end{bmatrix}$$

u_{LCIV} is the input matrix related to the voltage control loop which is obtained as:

$$u_{LCIV} = -K\, x_{LC} + \begin{bmatrix} k_I \\ 0 \end{bmatrix} \gamma \tag{20}$$

where γ is the integrator output given as:

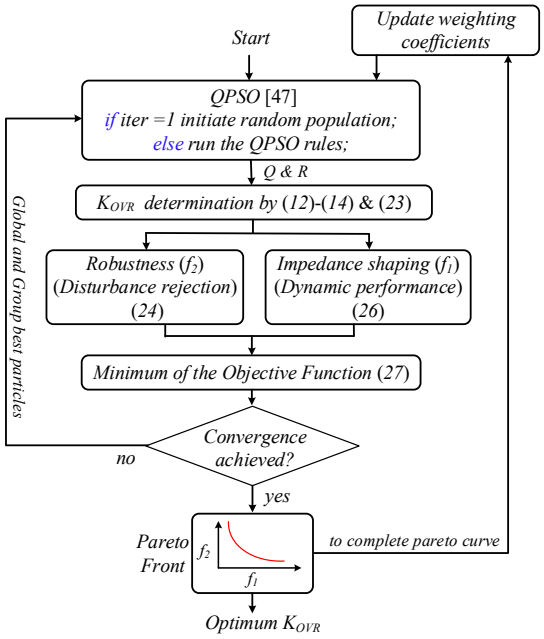

Fig. 4. The OVR optimization process; flowchart of the optimal K_{OVR} determination.

$$\dot{\gamma} = v_{odref} - v_{od} \tag{21}$$

and the matrix K is given as:

$$K = \begin{bmatrix} k_{11} & k_{12} & k_{13} & k_{14} \\ k_{21} & k_{22} & k_{23} & k_{24} \end{bmatrix} \tag{22}$$

u_{LCOC} is the input matrix related to the output current, which is regarded as disturbance. The augmented state space of OVR is derived as:

$$\begin{aligned} \dot{x}_{OVR} &= A_{OVR}\ x_{OVR} - B_{OVR}\ K_{OVR}\, x_{OVR} + B_{OVR,d}\, u_{OVR,d} \\ &= (A_{OVR} - B_{OVR}\ K_{OVR})\, x_{OVR} + B_{OVR,d}\, u_{OVR,d} \\ y_{OVR} &= C_{OVR}\, x_{OVR} \end{aligned} \tag{23}$$

where $x_{OVR} = \begin{bmatrix} x_{LC}^{\ T} & \gamma \end{bmatrix}^T$

$$A_{OVR} = \begin{bmatrix} A_{LC} & 0_{1\times 4} \\ -C_{LC} & 0 \end{bmatrix},\ B_{OVR} = \begin{bmatrix} B_{LCIV} \\ 0_{1\times 2} \end{bmatrix},\ K_{OVR} = \begin{bmatrix} K & \begin{bmatrix} -k_I \\ 0 \end{bmatrix} \end{bmatrix}$$

$$B_{OVR,d} = \begin{bmatrix} B_{LCOC} \\ 0_{1\times 2} \end{bmatrix},\ u_{OVR,d} = u_{LCOC}$$

$$C_{OVR} = \begin{bmatrix} C_{LC} & 0 \end{bmatrix},\ y_{OVR} = \Delta v_{od}$$

where $u_{OVR.d}$ is considered as a disturbance. From (23) the transfer function from the OVR's output voltage, Y_{OVR}, to the input disturbance, $U_{OVR.d}$, is developed in the frequency domain as follows:

$$G_{yu,d} = C_{OVR}\left(sI - A_{OVR} + B_{OVR}K_{OVR}\right)^{-1} B_{OVR,d} \tag{24}$$

where I is the identity matrix with appropriate dimension. It is worth noting the conventional PI-based VSI includes 8 state variables [42], while the proposed OVR includes 5 state variables, which considerably reduces the order of the power system containing a considerable number of DG units.

B. OVR Output Impedance

The control system of the OVR is represented in Fig. 3, and the mathematical model of the voltage control loop is given as:

$$v_{id} = -k_{11}\, i_{fd} - k_{12}\, i_{fq} - k_{13}\, v_{od} - k_{14}\, v_{oq} + \left(\frac{k_I}{s}\right)\left(v_{odref} - v_{od}\right) \tag{25a}$$

$$v_{iq} = -k_{21}\, i_{fd} - k_{22}\, i_{fq} - k_{23}\, v_{od} - k_{24}\, v_{oq} \tag{25b}$$

Similar equations like (1)-(2) & (7)-(8) are obtained for the OVR's output voltage using KVL. Plugging (7)-(8) and (25) into (1)-(2) for the OVR, the output voltage is developed as:

$$v_{oOVR}(s) = G_{OVR}(s)\ v_{odref} - Z_{odOVR}(s)\ i_{od} - Z_{oqOVR}(s)\ i_{oq} \tag{26}$$

A detailed version of (26) is given in Appendix B.

C. Determination of Optimal Q and R Matrices

In determining the Q & R matrices (and the feedback gain matrix K), we seek to achieve a desired impedance shaping as well as improving the robustness of the OVR in the disturbance rejection.

Objective Function (OF): the following OF is proposed to be minimized:

$$OF = \mathrm{W}_1 f_1 + \mathrm{W}_2 f_2 \tag{27}$$

$$f_1 = \left[\mathrm{W}_{11} f_{11} + \mathrm{W}_{12} f_{12} + \mathrm{W}_{13} f_{13}\right]$$

$$f_{11} = \left[\left\|\mathrm{M}_G - abs\left(G_{OVR}\right)\right\|_2^2 + \left\|0 - arg\left(G_{OVR}\right)\right\|_2^2\right]$$

$$f_{12} = \left[\left\|\mathrm{M}_d - abs\left(Z_{odOVR}\right)\right\|_2^2 + \left\|\phi_d - \frac{imag\left(Z_{odOVR}\right)}{real\left(Z_{odOVR}\right)}\right\|_2^2\right]$$

$$f_{13} = \left[\left\|\mathrm{M}_q - abs\left(Z_{oqOVR}\right)\right\|_2^2 + \left\|\phi_q - \frac{imag\left(Z_{oqOVR}\right)}{real\left(Z_{oqOVR}\right)}\right\|_2^2\right]$$

$$f_2 = \left[\left\|G_{yu,d}\right\|_\infty\right]$$

where *abs, arg, real* and *imag* denote the absolute value (magnitude), argument (phase angle), real, and imaginary parts, respectively; $\|.\|_2$ denotes 2-norm; M_G is the intended value for G_{OVR} magnitude; M_d and ϕ_d are the intended values for Z_{odOVR} magnitude and X/R ratio, respectively. M_q and ϕ_q are the intended values for Z_{oqOVR} magnitude and X/R ratio, respectively; $\mathrm{W}_{1,\ 2}$ and $\mathrm{w}_{11,\ } \mathrm{w}_{12,\ } \mathrm{w}_{13}$ are the weighting coefficients, and $\|.\|_\infty$ denotes the H_∞-norm:

$$\left\|G_{yu,d}\right\|_\infty = \sup_{0\le\omega<\infty} \sigma_{\max}\left[G_{yu,d}\left(j\omega\right)\right]$$

where $\sigma_{max}\left[G_{yu,d}(j\omega)\right]$ denotes the maximum singular value of $\mathrm{G}_{\mathrm{yu,d}}(j\omega)$.

Function f_1: it is developed, based on (26), to design the optimum output impedance shape (dynamic performance) of OVR:

- ***f_{11}***: M_G is considered 1 (0 dB). It makes the OVR to be a voltage regulator, which follows the reference value of the voltage magnitude.
- ***f_{12}***: the first and second terms specify the magnitude and phase angle (inductivity/resistivity) of the OVR output impedance, respectively. The selection of the optimal values for M_d and ϕ_d depends on the OVR's application, control targets and impedance characteristics of the grid. This issue is investigated in the second part of the paper and optimal impedance shaping is proposed to achieve the OVR's optimal dynamic performance.
- ***f_{13}***: it specifies the magnitude and phase angle of Z_{oqOVR}, which is included to remove negative damping and

present a damping factor for the reactive current.

Function f_2: it is developed based on the transfer function from the OVR's input disturbance to output voltage (24) given from the state space model. Minimizing the H_∞-norm of the transfer function, minimizes the effect (of the worst case) from the disturbance to the controlled output and thus improves the robustness of the system in rejecting disturbances caused by load variations.

Optimization: It is not an easy task to do the optimization due to the nonlinearity and multi-objectivity of the *OF*. Therefore, quantum-particle swarm optimization (QPSO) is developed in this paper.

The heuristic PSO method has become popular to solve the optimization problems in the engineering field [18], [46], and QPSO has been proposed to improve PSO convergence to the global optimum point [47]. Pareto is applied to QPSO to address the multi-objective of the proposed *OF*. The optimization flowchart is depicted in Fig. 4. First QPSO is adopted to optimize the OF for different weighting factors. Then, Pareto front is drawn to implement tradeoff between the objective functions (f_1 and f_2). Then final solution is selected from the Pareto front by the decision maker considering some constraints on the components of the objective function, for example that f_{11}, f_{12}, f_{13}, and f_2 should be lower than some assigned values determined during the design phase according to some requirements of the problem, which is discussed in the second part of the paper.

The control challenge related the method is that the optimization process for the feedback gain adjustment is time-consuming in case of real-time applications when the impedance shaping intended to be tuned adaptively. Nevertheless, since the robustness of the control system in disturbance rejection is secured in the proposed OF through f_2, the appropriate dynamic performance of the OVR is secured in a wide range of operating points, and thus the requirement of the real-time (on-line) optimization process, in order to take load and grid (grid's parameters and topology) variations into account, is eliminated. This issue is discussed in the second part of the paper where the optimal impedance shaping for different applications is presented.

IV. Numerical and Simulation Results

In this section, the effectiveness of the proposed OVR is evaluated via numerical examples and simulations in MATLAB/Simulink and using the Simscape toolbox. The electrical parameters and converter characteristics are given in Table I. The control parameters of the PI-based VSI are taken from [39], which are developed to get the best dynamic performance.

A. Optimization

For this case study, M_d and ϕ_d (phasors of the Z_{odOVR}) are considered 1 Ω and 7, respectively[3]. Based on (26) and considering the phase angle of i_{oq} is -90^0, the $Z_{oqOVR}\,i_{oq}$ term can be regarded as positive damping provided that the Z_{oqOVR} exhibits inductive characteristics, i.e. ϕ_q be larger than 6. To this end, the M_q and ϕ_q (phasors of the Z_{oqOVR}) are considered 0.1 Ω and 7, respectively.

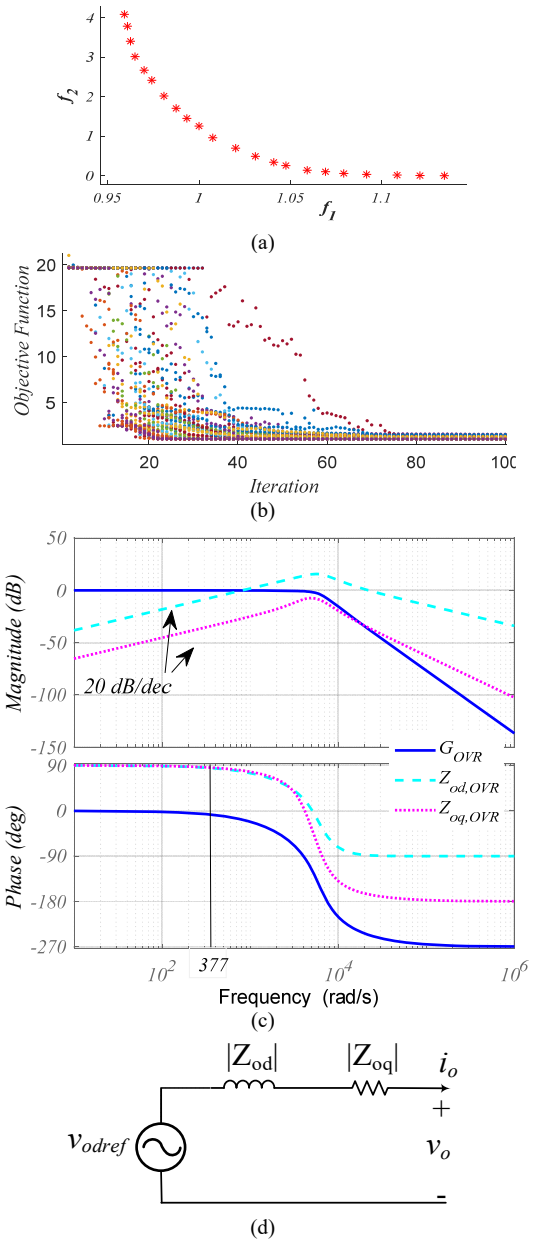

Fig. 5. Numerical results: (a) Pareto front; (b) convergence of the optimization algorithm after several runs; (c) bode plot of the OVR output impedance; (d) equivalent circuit model.

The weighting coefficients w_{11}, w_{12}, w_{13} are fixed to 1, 10, 5, respectively, while W_1 and W_2 are changing between 0-1, so that $W_1+W_2=1$, in order to achieve the Pareto front. The selected values of W_1 and W_2 given from the Pareto curve are 0.75 and 0.25, respectively. A global optimum solution is achieved after several runs of the optimization process, which is given in Fig. 5(a) and (b). The feedback gain matrix obtained from the optimization process, Fig. 4, is given as follows:

$$K_{OVR} = \begin{bmatrix} 14.39 & 00.52 & 01.99 & 00.18 & 5525 \\ 00.52 & 10.17 & 00.22 & 00.02 & 0000 \end{bmatrix}$$

The bode plots of $G_{OVR}(s)$, $Z_{odOVR}(s)$, and $Z_{oqOVR}(s)$, for OVR with electrical parameters given in Table I, are shown in Fig. 5(c). The magnitude and phase angle of $G_{OVR}(s)$ are 0.99 and -9°, respectively, which makes the OVR an ideal voltage source equal to v_{odref}. The phasor of Z_{odOVR} at the operating angular frequency is 0.95∠82°, by which the X/R

[3] Yet finding an optimal impedance shaping, based on the IIDGs application, remains as an open topic, which is studied in the second part of the paper. Here we are interested if the optimization method can produce a feedback gain matrix based on the defined output impedance.

ratio of output impedance is 6.80. The phasor of Z_{oqOVR} is roughly $0.065\angle 79^{o}$. The equivalent circuit model of the OVR is depicted in Fig. 5(d). It is worth to note that the output impedance is presented to model the dynamical performance of the OVR and output current does not cause a voltage drop over the output impedance so that v_o=v_{odref} at steady states in loading conditions. So, the voltage drop, which is the main drawback of the virtual impedance loop is eliminated.

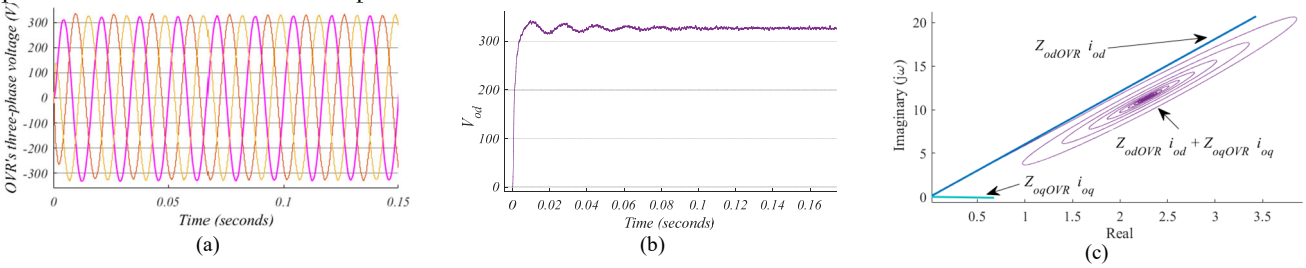

Fig. 6. OVR performance under voltage regulation: (a) three-phase voltage; (b) direct component of the voltage; (c) output impedance behavior.

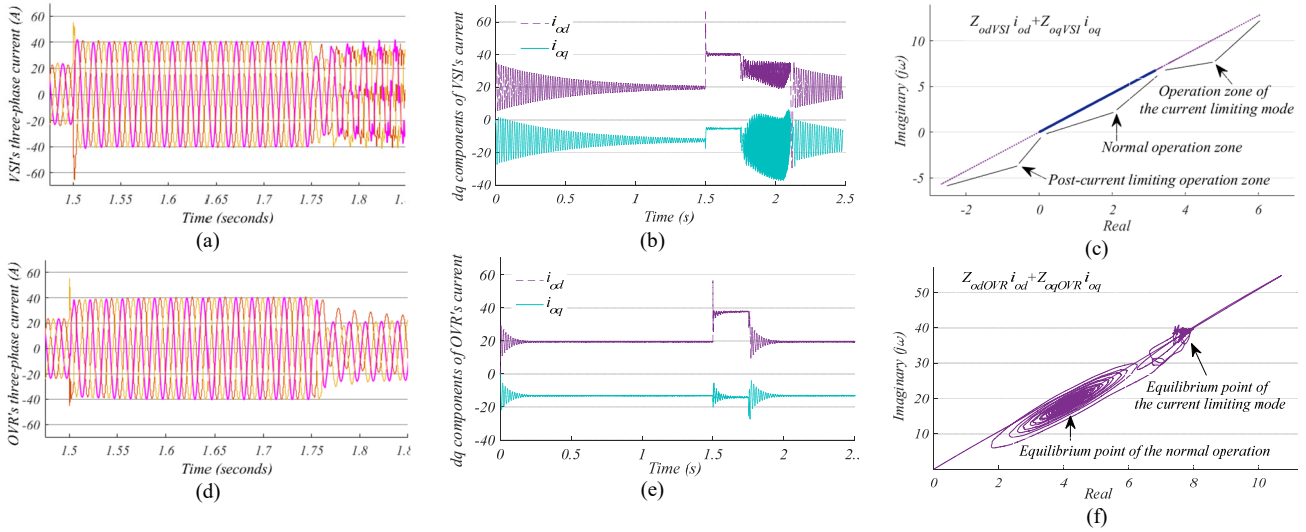

Fig. 7. OVR performance in current limiting mode, a balanced three-phase to ground fault occurs at t = 1.5 - 1.75 (seconds): (a) VSI's output three-phase current; (b) the *d-q* components of the VSI's output current; (c) VSI's output impedance behavior; (d) OVR's output three-phase current; (e) the *d-q* components of the OVR's output current; (f) OVR's output impedance behavior.

B. Simulation Results

The assessment practice includes voltage regulation and current limiting. The OVR is connected to the load bus via an interconnecting power line (Z_{line}=0.050+*j*0.056) and the load value is 10+j6 kVA.

Voltage regulation: the performance of a stand-alone OVR in voltage regulation is depicted in Fig. 6, including the three-phase output voltage waveform and the direct component, which is fixed to the nominal value, V_{od} = 326 (V). The output impedance behavior of the OVR is depicted in Fig. 6(c) where the dynamics of the OVR's virtual voltage drop is shown. $Z_{odOVR}(s)i_{od}(s)$ causes a voltage drop alongside the quadrature axis, which makes the output impedance of the OVR dominantly inductive. $Z_{oqOVR}(s)\ i_{oq}(s)$ participates in voltage drop along with direct component with roughly zero phase angle which provides a positive virtual damping for the OVR control system. Since Z_{odOVR} is much larger than Z_{oqOVR}, OVR preserves its inductivity in variety of loading conditions with different power factors.

Fault-ride through: In case of the PI-based VSI, the current limiting can be realized by including a current limiter in the VSI's control system [40]. In the case of the OVR, impedance shaping can be adopted for executing current limiting. To this end, a state feedback gain matrix (K_{OVRcl}) is designed for short-circuit situations and is held in a look-up table. When the OVR's current exceeds the threshold, feedback gain matrix switches to K_{OVRcl}. In designing the K_{OVRcl}, a large resistive-inductive output impedance could be considered for the OVR to provide current limiting while preserving the nature of the OVR's output impedance when the IIDG unit is invoked to a large disturbance. This issue is critical in order to stabilize a stand-alone OVR or an autonomous MG when IIDG units switch to the current limiting mode, which is investigated in more details in the second part of the paper. It also helps to design appropriate protection scheme [16]. The recommended feedback gain matrix for current limiting (K_{OVRcl}) is given as follows:

$$K_{OVRcl}=\begin{bmatrix}1.44 & 0.05 & 0.2 & 0.02 & 00\\ 0.05 & 1.01 & 0.02 & 00.00 & 00\end{bmatrix}$$

It worth noting that although the integrator gain (k_I) in K_{OVRcl} is zero, the integrator output is not reset (it is not zero) during current limiting mode to preserve voltage regulation during/after fault. It also avoids the integrator saturation during current limiting which is the common issue of the PI-based VSIs [48].

Figs. 7 compares the performance of the OVR with the performance of the conventional VSI when a balanced three-phase to ground fault happens at the load bus at t = 1.5 (s) and it is removed at t = 1.75 (s). Some important observations emerge from Fig. 7:

1) The OVR is more successful in limiting the initial current spark (which is harmful to semi-conductive switches) when the fault appears;

2) Comparing Figs. 7 (b) and (e) reveals a significant improvement in the dynamic performance of the OVR in comparison to the VSI;

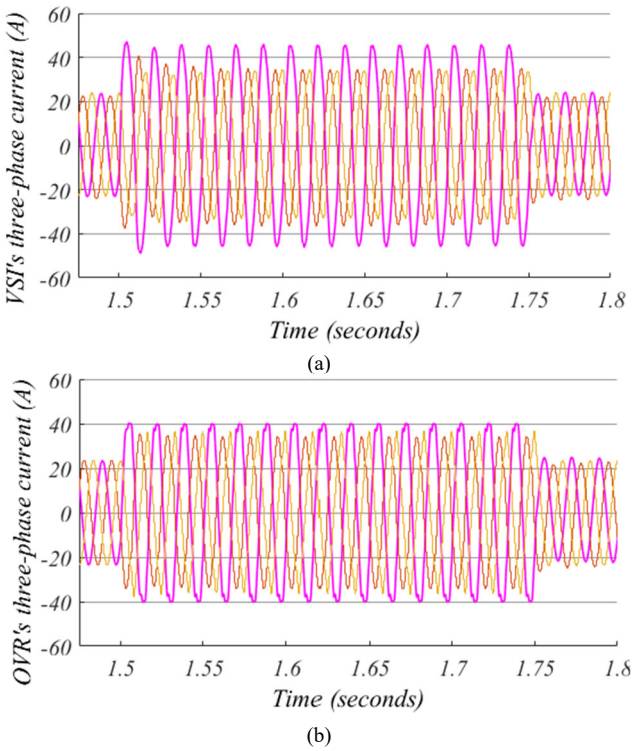

Fig. 8. OVR performance in current limiting mode, an unbalanced single-phase (phase a) to ground fault occurs at t = 1.5 - 1.75 (seconds): (a) VSI's output three-phase current; (b) OVR's output three-phase current;

3) The OVR control system preserves its impedance shape/inductivity in the current limiting mode which is vital for stability issues;

4) As expected, the output impedance of VSI is not purely inductive and not large enough to be effective. Besides, since Z_{oq} of the VSI is negligible, and thus due to lack of sufficient positive damping for reactive current, there is not a specific/same equilibrium point for VSI's pre/post current limiting mode. This may put the VSI into an operating zone with negative damping and may make the VSI unstable, see Fig. 7(c). This issue may lead to circulating current among parallel VSIs in an autonomous MG when inverters operate at the current limiting mode due to a fault or a large disturbance. In this situation, VSIs reveal different (even maybe capacitive) output impedance characteristics which diffuse into the power network [17] and thus coupling the *f-P* and *V-Q* droop controllers leads to instability of the MG. The authors are currently working on the issue to provide mathematical support for this idea using the Lyapunov nonlinear/direct method.

The performance of the OVR in current limiting in the presence of an unbalanced single-phase to ground fault, which is the most common fault type in the power systems, is evaluated in Fig. (8). The conventional VSI fails to limit current within the permitted band, I_{MAX} = 40 (A). The detailed analysis of the PI-based VSI's performance in unbalanced conditions can be found in [40]. On the other hand, the OVR successfully limits the output current within the tolerable band, which is essential for the fault ride-through of IIDG units, without including any extra control part. Although the current waveform is distorted, it can be solved by using a notch filter to filter out the oscillatory terms with angular frequency twice the grid frequency (2ω) [49].

V. Conclusion

In this paper, the importance of impedance shaping of IIDG units in stabilizing the modern power systems and autonomous MGs have been investigated. To this end, a new control system based on the impedance shaping, called optimal voltage regulator (OVR), has been proposed for controlling IIDG units. The optimality refers to the regulation process due to targeting optimal impedance shaping which is achieved through state feedback gain adjustment via the optimal LQR method. Moreover, the control structure has been designed in an optimal form to facilitate the appropriate/effortless impedance shaping.

The OVR can improve the dynamic performance and stability margins and reduce the order and complexity of the modern power systems. Moreover, fault-ride through is also provided by the OVR with appropriate impedance shaping.

Nevertheless, optimal selection of output impedance depends on the application of OVR and also on the impedance characteristic of the grid at point where the OVR is located. Hence, the OVR's optimal impedance shaping, which is specified based on the OVR's application (whether as a grid-connected inverter or as grid-forming in autonomous networked MGs) along with OVR performance in dealing with unbalanced/harmonic loads are investigated in the second part of the paper.

Appendix A

The PI-based VSI Output Impedance

The output voltage of a PI-based VSI is given as:

$$v_o = G(s)\, v_{odref} - Z_{od}(s)\, i_{od} - Z_{oq}(s)\, i_{oq}$$

where

$$G(s) = Num_0 / Den$$

$$Z_{od}(s) = Num_d / Den$$

$$Z_{oq}(s) = Num_q / Den$$

$$Den = \sum_{i=1}^{9} D_{(10-i)}\, s^{(i-1)}$$

$$D_1 = \left(C_f L_f\right)^2$$

$$D_2 = 2X\, C_f L_f$$

$$D_3 = X^2 + 2Y\, C_f L_f + \left(C_f\, L_f \omega_0\right)^2$$

$$D_4 = 2\left[X\, Y + C_f L_f\, Z + \omega_0^2 C_f^2 R_f L_f\right]$$

$$D_5 = 2X\, Z + Y^2 + 2C_f L_f k_{ic} k_{iv} + \left(C_f R_f \omega_0\right)^2$$

$$D_6 = 2\left[X\, k_{ic}\, k_{iv} + Y Z\right]$$

$$D_7 = Y\left(k_{ic}\, k_{iv}\right) + k_{pc} k_{vv} k_{ic} k_{iv} + Z^2$$

$$D_8 = 2\, Z\, k_{ic}\, k_{iv}$$

$$D_9 = \left(k_{ic}\, k_{iv}\right)^2$$

$$Num_0 = \sum_{i=1}^{7} N_{(8-i)}\, s^{(i-1)}$$

$$N_1 = C_f L_f k_{pc} k_{pv}$$

$$N_2 = X\, k_{pc} k_{pv} + Y\, C_f L_f$$

$$N_3 = X\,Z + Y\,k_{pc}k_{pv} + C_f L_f k_{ic}\,k_{iv}$$

$$N_4 = X\,k_{ic}k_{iv} + Z\left(Y + k_{pc}\,k_{pv}\right)$$

$$N_5 = Y\,k_{ic}\,k_{iv} + k_{pc}k_{pv}k_{ic}k_{iv} + Z^2$$

$$N_6 = 2Z\,k_{ic}\,k_{iv}$$

$$N_7 = \left(k_{ic}\,k_{iv}\right)^2$$

$$Num_d = \sum_{i=2}^{8} N_{d(9-i)}\,s^{(i-1)}$$

$$N_{d1} = \left(C_f\,L_f\right)^2$$

$$N_{d2} = L_f\,X + C_f\,L_f\left(R_f + k_{pc}(1-F)\right)$$

$$N_{d3} = \left(R_f + k_{pc}(1-F)\right)X + L_f Y + C_f\,L_f\,k_{ic}(1-F)$$

$$N_{d4} = k_{ic}(1-F)X + \left(R_f + k_{pc}(1-F)\right)Y + L_f\,Z$$

$$N_{d5} = L_f\,k_{ic}\,k_{iv} + k_{ic}(1-F)Y + \left(R_f + k_{pc}(1-F)\right)Z$$

$$N_{d6} = k_{ic}\,k_{iv}\left(R_f + k_{pc}(1-F)\right) + k_{ic}(1-F)Z$$

$$N_{d7} = k_{ic}^{\ 2}\,k_{iv}(1-F)$$

$$Num_q = \sum_{i=4}^{7} N_{q(8-i)}\,s^{(i-1)}$$

$$N_{q1} = \omega_0 C_f L_f^2$$

$$N_{q2} = C_f\,L_f\,\omega_0\left(2R_f + k_{pc}(1-F)\right)$$

$$N_{q3} = C_f\,R_f\,\omega_0\left(R_f + k_{pc}(1-F)\right) + C_f\,L_f\,\omega_0\,k_{ic}(1-F)$$

$$N_{q4} = C_f\,R_f\,\omega_0\,k_{ic}(1-F)$$

and

$$X = \left(C_f\,k_{pc} + C_f\,R_f\right)$$

$$Y = \left(C_f\,k_{ic} + k_{pc}k_{pv}\right)$$

$$Z = \left(k_{ic}\,k_{pv} + k_{pc}\,k_{iv}\right)$$

APPENDIX *B*
The OVR Output Impedance

The output voltage of OVR I s given as:

$$v_{oOVR}(s) = G_{OVR}(s)\,v_{odref} - Z_{odOVR}(s)\,i_{od} - Z_{oqOVR}(s)\,i_{oq}$$

where

$$G_{OVR}(s) = Num_{0OVR} / Den_{OVR}$$

$$Z_{od,OVR}(s) = Num_{dOVR} / Den_{OVR}$$

$$Z_{oq,OVR}(s) = Num_{qOVR} / Den_{OVR}$$

$$Den_{OVR} = \sum_{i=1}^{6} D_{OVR(7-i)}\,s^{(i-1)}$$

$$D_{OVR1} = \left(C_f\,L_f\right)^2$$

$$D_{OVR2} = C_f^{\ 2}\,L_f\left(k_{11} + k_{22} + 2R_f\right)$$

$$\begin{aligned} D_{OVR3} = C_f[&C_f(R_f^{\ 2} + R_f(k_{11}+k_{22}) + k_{11}k_{22} - k_{12}k_{21}) \\ &+ C_f L_f\omega_0(k_{21} - k_{12} + 2L_f\omega_0) \\ &+ L_f\,(2 + k_{13} + k_{24})] \end{aligned}$$

$$\begin{aligned} D_{OVR4} = C_f[&2R_f + k_{11} + k_{22} + k_{11}k_{24} - k_{12}k_{23} + k_{13}k_{22} - k_{14}k_{21} \\ &+ L_f\,(k_I - 2k_{14}\omega_0 + 2k_{23}\omega_0) + R_f(k_{13} + k_{24}) \\ &+ C_f L_f\omega_0^2(k_{11} + k_{22} + 2R_f)] \end{aligned}$$

$$\begin{aligned} D_{OVR5} = 1 &+ k_{13} + k_{24} + k_{13}k_{24} - k_{14}k_{23} + C_f L_f\omega_0^{\ 2}[-2 - k_{13} - k_{24}] \\ &+ C_f^{\ 2}\omega_0^{\ 2}[k_{11}k_{22} - k_{12}k_{21} + R_f(k_{11} + k_{22}) \\ &+ R_f^{\ 2} - L_f\omega_0(k_{21} - k_{12}) + L_f^{\ 2}\omega_0^{\ 2}] \\ &+ C_f[k_I k_{22} + k_I R_f + \omega_0(k_{12} - k_{21} + k_{11}k_{23} \\ &- k_{13}k_{21} + k_{12}k_{24} - k_{14}k_{22} + R_f(k_{23} - k_{14}))] \end{aligned}$$

$$D_{OVR6} = k_i\left[1 + k_{24} - C_f\omega_0\left(k_{21} + L_f\omega_0\right)\right]$$

$$Num_{0OVR} = \sum_{i=1}^{3} N_{OVR(4-i)}\,s^{(i-1)}$$

$$N_{OVR1} = k_I\,C_f L_f$$

$$N_{OVR2} = k_I C_f\,(k_{22} + R_f)$$

$$N_{OVR3} = k_I\left[1 + k_{24} - C_f\omega_0(k_{21} + L_f\omega_0)\right]$$

$$Num_{dOVR} = \sum_{i=2}^{5} N_{dOVR(6-i)}\,s^{(i-1)}$$

$$N_{dOVR1} = C_f L_f^{\ 2}$$

$$N_{dOVR2} = C_f L_f\left(k_{11} + k_{22} + 2R_f\right)$$

$$\begin{aligned} N_{dOVR3} = L_f(1 + k_{24}) + C_f[&k_{11}k_{22} - k_{12}k_{21} + R_f(k_{11} + k_{22}) \\ &+ R_f^{\ 2} + L_f\omega_0(k_{21} - k_{12} + L_f\omega_0)] \end{aligned}$$

$$N_{dOVR4} = k_{11} + k_{11}k_{24} - k_{14}k_{21} + R_f(1 + k_{24}) - L_f\omega_0 k_{14}$$

$$Num_{qOVR} = \sum_{i=2}^{4} N_{qOVR(5-i)}\,s^{(i-1)}$$

$$N_{qOVR1} = C_f L_f^{\ 2}\omega_0$$

$$N_{qOVR2} = -L_f k_{14} + C_f L_f\omega_0\left[k_{11} + k_{22} + 2R_f\right]$$

$$\begin{aligned} N_{qOVR3} = k_{12} &+ k_{12}k_{24} - k_{14}k_{22} - R_f k_{14} - L_f\omega_0(1 + k_{24}) \\ &+ C_f\omega_0[k_{11}k_{22} - k_{12}k_{21} + R_f(k_{11} + k_{22}) + R_f^{\ 2}] \\ &+ C_f L_f\omega_0^{\ 2}[k_{21} - k_{12} + L_f\omega_0] \end{aligned}$$

REFERENCES

[1] H. Farzin, M. Fotuhi-Firuzabad, and M. Moeini-Aghtaie, "Reliability studies of modern distribution systems integrated with renewable generation and parking lots," *IEEE Trans. on Sustain. Energy,* vol. 8, no. 1, pp. 431-440, 2016.

[2] F. Blaabjerg, Z. Chen, and S. B. Kjaer, "Power electronics as efficient interface in dispersed power generation systems," *IEEE Trans. on Power Electron.,* vol. 19, no. 5, pp. 1184-1194, 2004.

[3] A. Timbus, *et al.*, "Evaluation of current controllers for distributed power generation systems." *IEEE Trans. on Power Electron.,* vol. 24, no. 3, 654-664, 2009.

[4] R. Teodorescu, F. Blaabjerg, M. Liserre, and P. C. Loh, "Proportional-resonant controllers and filters for grid-connected voltage-source converters," *IEE Proceedings-Elect. Power Appl.,* vol. 153, no. 5, pp. 750-762, 2006.

[5] H. Karimi, E. J. Davison, and R. Iravani, "Multivariable servomechanism controller for autonomous operation of a distributed generation unit: Design and performance evaluation," *IEEE Trans. on Power Syst.,* vol. 25, no. 2, pp. 853-865, 2009.

[6] M. N. Marwali, and Ali Keyhani, "Control of distributed generation systems-Part I: Voltages and currents control," *IEEE Trans. on Power Electron.,* vol.19, no. 6, pp. 1541-1550, 2004.

[7] T. L. Tai and J. S. Chen, “UPS inverter design using discrete-time sliding mode control scheme,” *IEEE Trans. Ind. Electron.*, vol. 49, no. 1, pp. 67–75, Feb. 2002.

[8] D. E. Kim and D. C. Lee, “Feedback linearization control of three-phase UPS inverter systems,” *IEEE Trans. Ind. Electron.*, vol. 57, no. 3, pp. 963–968, Mar. 2010.

[9] S. Dasgupta, *et al*.,, “Lyapunov function-based current controller to control active and reactive power flow from a renewable energy source to a generalized three-phase microgrid system,” *IEEE Trans. Ind. Electron.*, vol. 60, no. 2, pp. 799–813, 2013.

[10] Y. Shan, J. Hu, Z. Li, and J. M. Guerrero, "A model predictive control for renewable energy based ac microgrids without any PID regulators," *IEEE Trans. on Power Electron.,* vol. 33, no. 11, pp. 9122-9126, 2018.

[11] C. Xia, T. Liu, T. Shi, and Z. Song, "A simplified finite-control-set model-predictive control for power converters," *IEEE Trans. on Ind. Informa.,* vol. 10, no. 2, pp. 991-1002, 2014.

[12] K. De Brabandere, B. Bolsens, J. V. d. Keybus, A. Woyte, J. Driesen, R. Belmans. "A voltage and frequency droop control method for parallel inverters." *IEEE Trans. on Power Electron.,* vol. 22, no. 4, pp. 1107-1115, Jul. 2007.

[13] Q. C. Zhong, G. Weiss, “Synchronverters: Inverters that mimic synchronous generators,” *IEEE Trans. on Ind. Electron.,* vol. 58, no. 4, pp. 1259-1267, 2011.

[14] M. Eskandari, L. Li, and M. H. Moradi. "Decentralized Optimal Servo Control System for Implementing Instantaneous Reactive Power Sharing in Microgrids." *IEEE Trans. on Sustain. Energy*, vol. 9, no. 2, 525-537, 2018.

[15] J. Rocabert, A. Luna, F. Blaabjerg, and P. Rodriguez, "Control of power converters in AC microgrids," *IEEE Trans. on Power Electron.,* vol. 27, no. 11, pp. 4734-4749, 2012.

[16] B. Mahamedi, J. G. Zhu, M. Eskandari, L. Li, and A. Mehrizi-Sani, "Analysis of Fault Response of Inverter-Interfaced Distributed Generators in Sequence Networks," in *2018 IEEE Ind. Appl. Society Annu.Meeting (IAS)*, pp. 1-9, 2018.

[17] P. Monshizadeh, N. Monshizadeh, C. De Persis, and A. van der Schaft, "Output impedance diffusion into lossy power lines," *IEEE Trans. on Power Syst.,* vol. 34, no. 3, pp. 1659-1668, 2018.

[18] M. H. Moradi, M. Eskandari, and S. M. Hosseinian, "Operational strategy optimization in an optimal sized smart microgrid," *IEEE Trans. on Smart Grid,* vol. 6, no. 3, pp. 1087-1095, 2015.

[19] B. Zhao, *et al.*, "Operation optimization of standalone microgrids considering lifetime characteristics of battery energy storage system," *IEEE Trans. on Sustain. Energy,* vol. 4, no. 4, pp. 934-943, 2013.

[20] J. M. Guerrero, J. C. Vasquez, J. Matas, L. G. De Vicuña, and M. Castilla, "Hierarchical control of droop-controlled AC and DC microgrids—A general approach toward standardization," *IEEE Trans. on Ind. Electron.,* vol. 58, no. 1, pp. 158-172, 2011.

[21] J. Liu, Y. Miura, H. Bevrani, and T. Ise, "Enhanced virtual synchronous generator control for parallel inverters in microgrids," *IEEE Trans. on Smart Grid,* vol. 8, no. 5, pp. 2268-2277, 2016.

[22] M. Eskandari, L. Li, M. H. Moradi, P. Siano, and F. Blaabjerg, "Active power sharing and frequency restoration in an autonomous networked microgrids," *IEEE Trans. on Power Syst.,* vol. 34, no. 6, pp. 4706-4717, 2019.

[23] P. H. Divshali, A. Alimardani, S. H. Hosseinian, and M. Abedi, "Decentralized cooperative control strategy of microsources for stabilizing autonomous VSC-based microgrids," *IEEE Trans. on Power Syst.,* vol. 27, no. 4, pp. 1949-1959, 2012.

[24] X. Tang, X. Hu, N. Li, W. Deng, and G. Zhang, "A novel frequency and voltage control method for islanded microgrid based on multi energy storages," *IEEE Trans. on Smart Grid,* vol. 7, no. 1, pp. 410-419, 2014.

[25] M. Eskandari, L. Li, M. H. Moradi, F. Wang, and F. Blaabjerg, "A Control System for Stable Operation of Autonomous Networked Microgrids," *IEEE Trans. on Power Del.,* 2019.

[26] M. Cespedes, and Jian Sun, "Impedance Modelling and Analysis of Grid-Connected Voltage-Source Converters," *IEEE Trans. on Power Electron.,* vol. 29, no. 3, pp. 1254-1261, 2013.

[27] B. Wen, D. Dong, D. Boroyevich, R. Burgos, P. Mattavelli, and Z. Shen, "Impedance-based analysis of grid-synchronization stability for three-phase paralleled converters," *IEEE Trans. on Power Electron.,* vol. 41, no. 1, pp. 26-38, 2015.

[28] D. Lu, X. Wang, and F. Blaabjerg, "Impedance-based analysis of DC-link voltage dynamics in voltage-source converters," *IEEE Trans. on Power Electron.,* vol. 34, no. 4, pp. 3973-3985, 2019.

[29] X. Feng, J. Liu, and F. C. Lee, "Impedance specifications for stable DC distributed power systems," *IEEE Trans. on Power Electron.,* vol. 17, no. 2, pp. 157-162, 2002.

[30] J. Sun, "Impedance-based stability criterion for grid-connected inverters," *IEEE Trans. on Power Electron.,* vol. 26, no. 11, pp. 3075-3078, 2011.

[31] C. M.Wildrick, F. C. Lee, B. H. Cho, and B. Choi, “A method of defining the load impedance specification for a stable distributed power system,” *IEEE Trans. Power Electron.*, vol. 10, no. 3, pp. 280–285, Mar. 1995.

[32] A. Emadi, A. Khaligh, C. H. Rivetta, and G. A. Williamson, “Constant power loads and negative impedance instability in automotive systems: Definition, modeling, stability and control of power,” *IEEE Trans. Veh. Technol.*, vol. 55, no. 4, 1112–1125, 2006.

[33] S. D. Sudhoff, S. F. Glover, P. T. Lamm, D. H. Schmucker, and D. E. Delisle, “Admittance space stability analysis of power electronic systems,” *IEEE Trans. Aerosp. Electron. Syst.,* vol. 36, no. 3, pp. 965–973, Jul. 2000.

[34] J. Sun, "Small-signal methods for AC distributed power systems–a review," *IEEE Trans. on Power Electron.,* vol. 24, no. 11, pp. 2545-2554, 2009.

[35] X. Wang, Y. W. Li, F. Blaabjerg, and P. C. Loh, "Virtual-impedance-based control for voltage-source and current-source converters," *IEEE Trans. on Power Electron.,* vol. 30, no. 12, pp. 7019-7037, 2014.

[36] J. He, Y. *et al.*, “An Islanding Microgrid Power Sharing Approach Using Enhanced Virtual Impedance Control Scheme,” *IEEE Trans. on Power Electron.,* vol. 28, no. 11, pp. 5272-5282, 2013.

[37] M. Eskandari, L. Li, “Microgrid operation improvement by adaptive virtual impedance,” *IET Renew. Power Gen.,* vol. 13, no. 2, pp. 296-307, 2018.

[38] Y. W. Li and C. N. Kao, “An accurate power control strategy for power electronics-interfaced distributed generation units operating in a low voltage multibus microgrid,” *IEEE Trans. Power Electron.*, vol. 24, no. 12, pp. 2977–2988, Dec. 2009.

[39] N. Pogaku, M. Prodanovic, and T. C. Green, "Modeling, analysis and testing of autonomous operation of an inverter-based microgrid," *IEEE Trans. on Power Electron.,* vol. 22, no. 2, pp. 613-625, 2007.

[40] B. Mahamedi, M. Eskandari, J. Fletcher, J. Zhu, “Sequence-Based Control Strategy With Current Limiting for the Fault Ride-Through of Inverter-Interfaced Ddistributed Generators,” *IEEE Trans. on Sustain. Energy*, vol. 11, no. 1, pp. 165-174, 2020.

[41] W. Yao, *et al.*, "Design and analysis of the droop control method for parallel inverters considering the impact of the complex impedance on the power sharing," *IEEE Trans. on Ind. Electron.,* vol. 58, no. 2, pp. 576-588, 2010.

[42] M. Eskandari, L. Li, M. H. Moradi, P. Siano “A Nodal Approach-based State-Space Model of Droop-Based Autonomous Networked Microgrid,” *Sustain. Energy, Grids and Networks,* vol. 18, p. 100216, 2019.

[43] J. M. Guerrero, L. G. De Vicuna, J. Matas, M. Castilla, J. Miret. "Output impedance design of parallel-connected UPS inverters with wireless load-sharing control." *IEEE Trans. on Ind. Electron.,* vol. 52, no. 4, pp. 1126-1135. 2005.

[44] W.-M. Guo, L.-H. Mu, and X. Zhang, "Fault models of inverter-interfaced distributed generators within a low-voltage microgrid," *IEEE Trans. on Power Del.,* vol. 32, no. 1, pp. 453-461, 2017.

[45] K. Ogata and Y. Yang, *Modern control engineering*. Prentice-Hall, 2002.

[46] Y. Shi, "Particle swarm optimization: developments, applications and resources," in *Proceedings of the 2001 congress on evolutionary computation (IEEE Cat. No. 01TH8546)*, 2001, vol. 1, pp. 81-86: IEEE.

[47] J. Sun, B. Feng, and W. Xu, "Particle swarm optimization with particles having quantum behavior," in *Proceedings of the 2004 congress on evolutionary computation (IEEE Cat. No. 04TH8753)*, 2004, vol. 1, pp. 325-331: IEEE.

[48] A. D. Paquette and D. M. Divan, "Virtual impedance current limiting for inverters in microgrids with synchronous generators," *IEEE Trans. on Ind. Applications,* vol. 51, no. 2, pp. 1630-1638, 2014.

[49] D. Shin, K.-J. Lee, J.-P. Lee, D.-W. Yoo, and H.-J. Kim, "Implementation of fault ride-through techniques of grid-connected inverter for distributed energy resources with adaptive low-pass notch PLL," *IEEE Trans. on Power Electron.,* vol. 30, no. 5, pp. 2859-2871, 2014.